STM JOURNALS

Journal of
Catalyst & Catalysis

ISSN: 2349-4344
Volume 11, Issue 3, 2024
September—December
DOI (Journal): 10.37591/JoCC

https://journals.stmjournals.com/jocc

Review JoCC

# Synthesis and Structural Characterization of Nanocrystalline $CeO_2$ and $Ce_{0.95}Cu_{0.05}O_2$ Solid Solution Catalysts: Properties and Applications

G.O. Obaiah[1,*], Chaithanya S.[2], M. Mylarappa[3]

***Abstract***

*The main study and the development of $CeO_2$ and Cu-doped $CeO_2$ nanocrystals containing transition-metal species are of crucial importance for understanding the preparation and fabrication of $CeO_2$ and Cu-doped $CeO_2$ nanoparticles by solution combustion technique to taken glycine as fuel. The structural properties of $Ce_{1-x}Cu_xO_2$ nanocrystals were examined by investigating the influence of cerium dioxide and Cu dopant ions. The $CeO_2$ single-phase cubic system was successfully incorporated with Cu ions using the co-precipitation technique, as confirmed by X-ray diffraction results. Field emission scanning electron microscopy and energy dispersive spectroscopy were used to evaluate the surface structure and crystallinity of the produced materials using various characterization techniques. The Ce-O stretching mode is the cause for the significant broad band in the Fourier transform infrared spectrum below 600 $cm^{-1}$, which confirms the synthesis of pure $CeO_2$. $CeO_2$ nanoparticles are a potential material for photocatalytic and optoelectronic applications because of their required structural and optical characteristics. Under ultraviolet light exposure, the photocatalytic properties of $CeO_2$ and Cu-doped $CeO_2$ nanoparticles were examined using Rose Bengal dye and Rose Bengal Cu/$CeO_2$. In a comparative investigation conducted with and without catalysts, $CeO_2$ and Cu-doped $CeO_2$ show exceptional photocatalytic activity by breaking down over 82% of the Rose Bengal-Cu/$CeO_2$ in 60-min intervals under ultraviolet light.*

**Keywords:** Mixed metal oxides, copper-doped ceria nanocomposites, heterogeneous catalysis, photocatalytic applications

## INTRODUCTION

Cerium (Ce) is a lanthanide rare-earth element found abundantly in the earth's crust. Cerium dioxide ($CeO_2$) has received widespread recognition for its numerous applications in a variety of industries due to its extended structural and optical properties [1]. $CeO_2$ has received serious consideration in catalytic area of environmental pollution control such as redox property, versatile acid-base catalytic chemistry, and excellent oxygen storage ability [2]. Doping or the incorporation of additives is effective strategies for enhancing the sulfur resistance of Ce-based catalysts, as evidenced by various applications [3]. This study describes the performance of Cu-doped $CeO_2$ ($Ce_{0.95}Cu_{0.05}O_2$) catalyst for synthesis at low temperature within a homogeneous mixture. A comprehensive investigation of both bulk and surface structures has been carried out to elucidate the relationship

***Author for Correspondence**
G.O. Obaiah
E-mail: obavasu@gmail.com

[1,2]Assistant Professor, Department of Chemistry, Karnataka State Open University, Mukhtagangotri Mysore, Karnataka, India
[3]Assistant Professor, Department of Chemistry, Bangalore University, Bengaluru, Karnataka, India

Received Date: October 19, 2024
Accepted Date: October 28, 2024
Published Date: December 26, 2024

**Citation:** G.O. Obaiah, Chaithanya S., M. Mylarappa. Synthesis and Structural Characterization of Nanocrystalline $CeO_2$ and $Ce_{0.95}Cu_{0.05}O_2$ Solid Solution Catalysts: Properties and Applications. Journal of Catalyst & Catalysis. 2024; 11(3): 29–38p.

 

between redox and catalytic characteristics of the active species. The effectiveness of $CeO_2$ in these applications arises from its capacity to exist in two oxidation states-cerous ($Ce^{3+}$) and ceric ($Ce^{2+}$) oxide-rendering it one of the most reactive redox binary metal oxides [4]. In addition, $CeO_2$ exhibits a lattice parameter that coincides closely with that of Si, thereby improving its potential for luminescent applications. $CeO_2$ based semiconductors demonstrate a wide band gap of 3.6 eV, maintain optical transparency in the visible light range, and display efficient luminescence in the UV spectrum [5]. These techniques make it easy to locate any foreign objects or disorders inside the structure because they are sensitive to molecular vibrations and the production of photons from electron transitions. Oxygen vacancy defects have been found to contribute to the enhanced oxygen storage capacity of Cu-doped $CeO_2$ [6–8].

In this study, porous nano catalysts of $CeO_2$ and Cu-doped $CeO_2$ were synthesized using a solution combustion method. The $Ce_{0.95}Cu_{0.05}O_2$ catalyst demonstrates outstanding characteristic properties and remarkable long-term stability. We utilized sophisticated characterization methods to explore the effects of copper doping on cerium dioxide and the structural defects present in $CeO_2$.The investigation of the structural activity relationships of Cu-doped $CeO_2$ catalysts aimed at improving catalytic performance across various applications.

## MATERIALS AND EXPERIMENTAL METHODS

### Materials

Ceric ammonium nitrate [$(NH_4)_2$ Ce $(NO_{3)6}$, 99.9%], copper nitrate [Cu $(NO_3)_2$ .$3H_2O$, 99.9%], palladium chloride [$PdCl_2$, 99%] and urea [$NH_2CONH_2$, 99.9%] were purchased from Sigma Aldrich.

### Synthesis of $CeO_2$ and $Ce_{0.95}Cu_{0.05}O_{2-\delta}$ Catalysts

The synthesis of single-phase compound was prepared using a single-step urea-assisted solution combustion method. The starting materials are Ceric ammonium nitrate, cupric nitrate and glycine as fuel. The synthesis of $CeO_2$ required a stoichiometric ratio of starting materials, specifically for the preparation of $Ce_{0.95}Cu_{0.05}O_{2-\delta}$, which was 9.92 mmol of ceric ammonium nitrate $(NH_4)_2Ce$ $(NO_3)_6$ and 10.902 mmol of glycine in a 300 mL crystallization salt container with the reactants dissolved in 15 mL of $H_2O$.

The stoichiometric ratio of starting materials were taken as 10.416 g of $(NH_4)_2Ce$ $(NO_3)_6$, 0.2416 g of Cu $(NO_3)_2.3H_2O$, 0.109 g of $PdCl_2$ and 10.902 mmol of glycine was utilized in a 300 mL crystallization salt container, with the reactants dissolved in 15 mL of $H_2O$, particularly for the preparation of $Ce_{0.95}Cu_{0.05}O_{2-\delta}$. The solution ignited to burn with a flame takes place once dehydration is completed to get the voluminous reliable product is obtained. The solid product was chosen for structural characterization.

## RESULTS AND DISCUSSION

### X-Ray Diffraction Analysis

X-ray diffraction (XRD) analysis of $CeO_2$ (Figure.1) was performed on a diffractometer with monochromatic CuKα radiation (λ = 0.15406 nm) in the range of Bragg angles (2θ) from 20°to 100° with a step scanning of 0.01° at a speed of 2 °/min. Qualitative X-ray analysis was carried out using a powder XRD database. Quantitative X-ray analysis was performed using the Rietveld method. In Figure 1, XRD pattern of $CeO_2$ shows nanocrystalline planes and the particle size was calculated using Debye-Scherer using Equation (1).

$$D = \frac{\lambda k}{\beta \cos \theta} \tag{1}$$

where $\lambda$ is wavelength in nm; $\beta$ is full width at half maximum in radians and $\theta$ represents Bragg angle in radians. The broadening in peaks can be easily detected at first glance confirming the nanocrystalline behavior of the particles. The indexing of the peaks, represented by the blue vertical lines marked below the XRD peaks, has shown the presence of (111), (200), (220), (311), (222), (400), (331), and (420)

 

planes. Bragg's reflections at allowed 2θ values, which correspond to the face-centered cubic crystal structure related to space group Fm-3m, possess $Ce^{4+}$ ions positioned at tetrahedral and $O^{2-}$ ions at octahedral lattice sites. The XRD patterns are index as anatase phase of $CeO_2$, and additionally, the physical phenomenon data were in good a correspondence with JCPDS Number 340394.

X-ray powder diffraction (PXRD) was used to ascertain the phase structure and average crystallite size of the suggested catalytic materials. These Cu-doped $CeO_2$ nanocomposites are shown in Figure 1. Diffraction peaks indicating the face-centered cubic phase of $CeO_2$ in the synthesized catalysts were found at 2θ = 33.2° (200), 28.2° (111), and 56.2° (311). This pattern corresponds to file number 65-2975 in JCPDS [9]. The XRD patterns of a reported ceria closely match the XRD peaks [10]. The peak at 47.6 (220) is used to identify CuO [11, 12]. The PXRD results showed that the nano-composites were highly crystalline, as seen by the conspicuous peaks. The cerium and cerium copper nano-composites had average crystalline diameters of 20.73 and 23.22 nm, respectively, according to calculations.

**Analysis of Fourier Transform Infrared Spectra**

Figure 2 displays the catalyst's Fourier transform infrared (FTIR) pattern. There are three distinct sections in the FTIR spectrum: 500 $cm^{-1}$, 1300–1800 $cm^{-1}$, and 3500–3000 $cm^{-1}$ [13]. OH adsorbed on the catalyst surface stretching in the O-H direction is indicated by the peaks at 3700 $cm^{-1}$. The stretching vibrations of OH are responsible for the enlargement of the absorption peak at 3446 $cm^{-1}$. The 1541 $cm^{-1}$ band is produced by the water H-O-H bending vibration mode. The third low wave number zone absorption below 500 $cm^{-1}$ may be related to the Ce-O and Cu-O stretching vibrational modes, which indicate oxide synthesis, because oxides form bonds in this region [14].

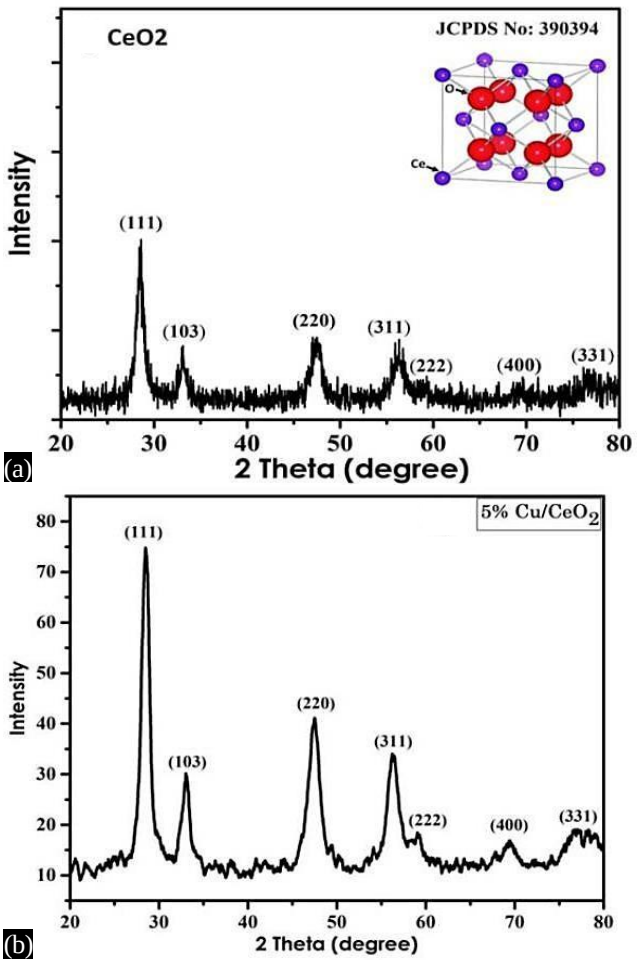


**Figure 1.** Powder X-ray diffraction (XRD) pattern of (a) $CeO_2$ and (b) 5% $Cu/CeO_2$ ($Ce_{0.95}Cu_{0.05}O_2$) catalysts.

 

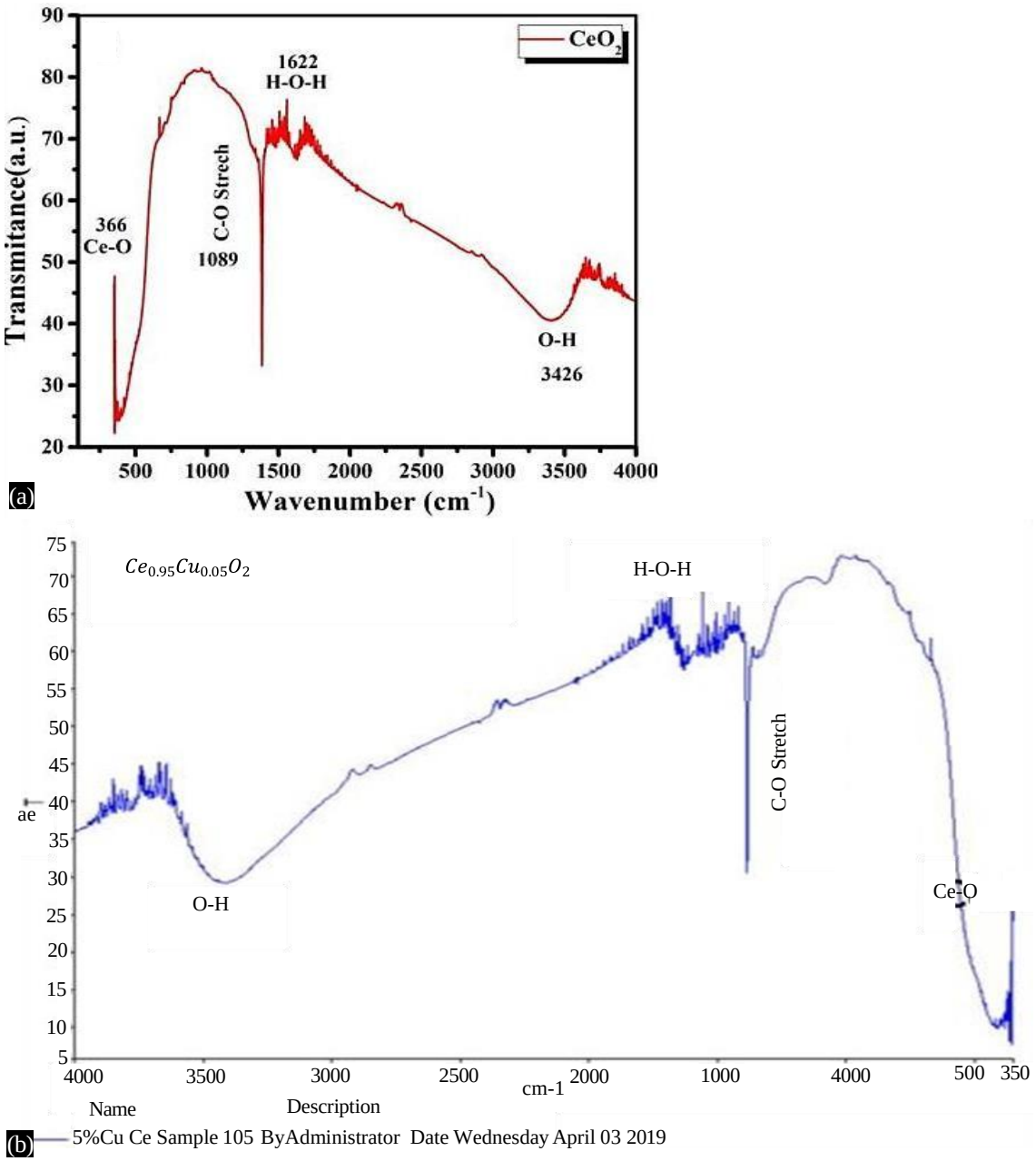


**Figure 2.** Fouries transform infrared (FTIR) spectra of (a) $CeO_2$, and (b) 5% Cu/$CeO_2$ ($Ce_{0.95}Cu_{0.05}O_2$).

**Scanning Electron Microscopy and Energy-Dispersive X-Ray Analysis**

The structure of cerium nano-composites and scanning electron microscopy (SEM) micrographs of the Cu-doped $CeO_2$ catalyst are shown in Figure 3. The micrograph shows the enormous clusters of little $CeO_2$ particles. Between 25 and 30 nm is the typical particle size [15, 16]. The photographs clearly show that these nanocomposites form a heterogeneous surface structure that enables catalysis, despite the fact that some agglomerations were visible.

The energy dispersive spectroscopy (EDS) and SEM was used to examine the elemental composition and surface morphology of the particles as shown in Figures 3 and 4. The EDS spectrum is displayed in Figure 4 which confirms the sample purity of as-synthesized composites. In Figure 4, cerium (Ce), copper (Cu), and oxygen (O) are the main constituents present in the nanocomposite as indicated in Table 1.

 

**Table 1.** Weight percentage of elements in $Cu/CeO_2$.

| Element | Weight (%) | Element | Weight (%) |
|---|---|---|---|
| O K | 15.11 | O K | 10.16 |
| Cu K | 1.51 | – | – |
| Ce L | 83.38 | Ce L | 89.84 |
| Total | 100.00 | Total | 100.00 |

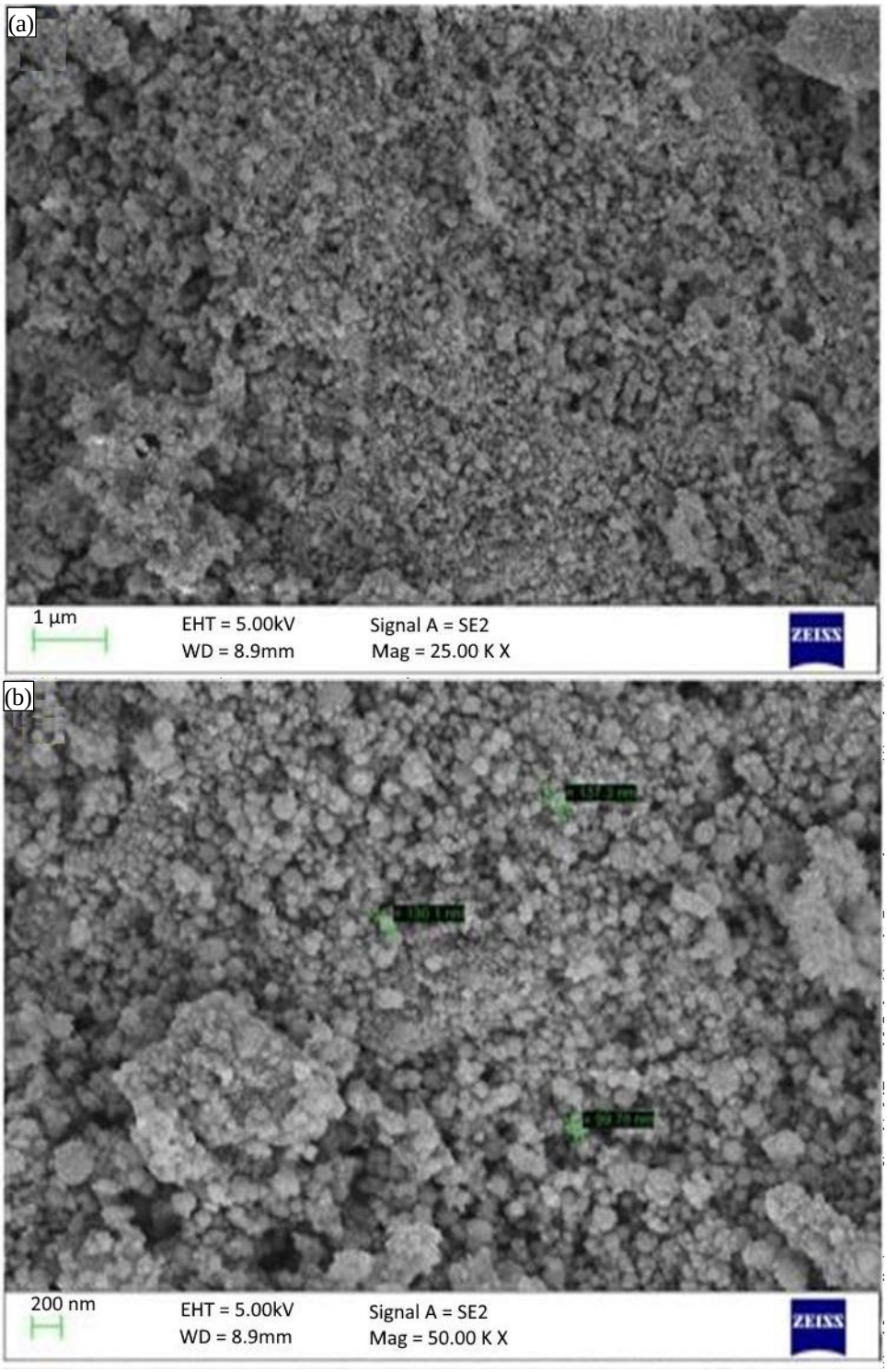


 

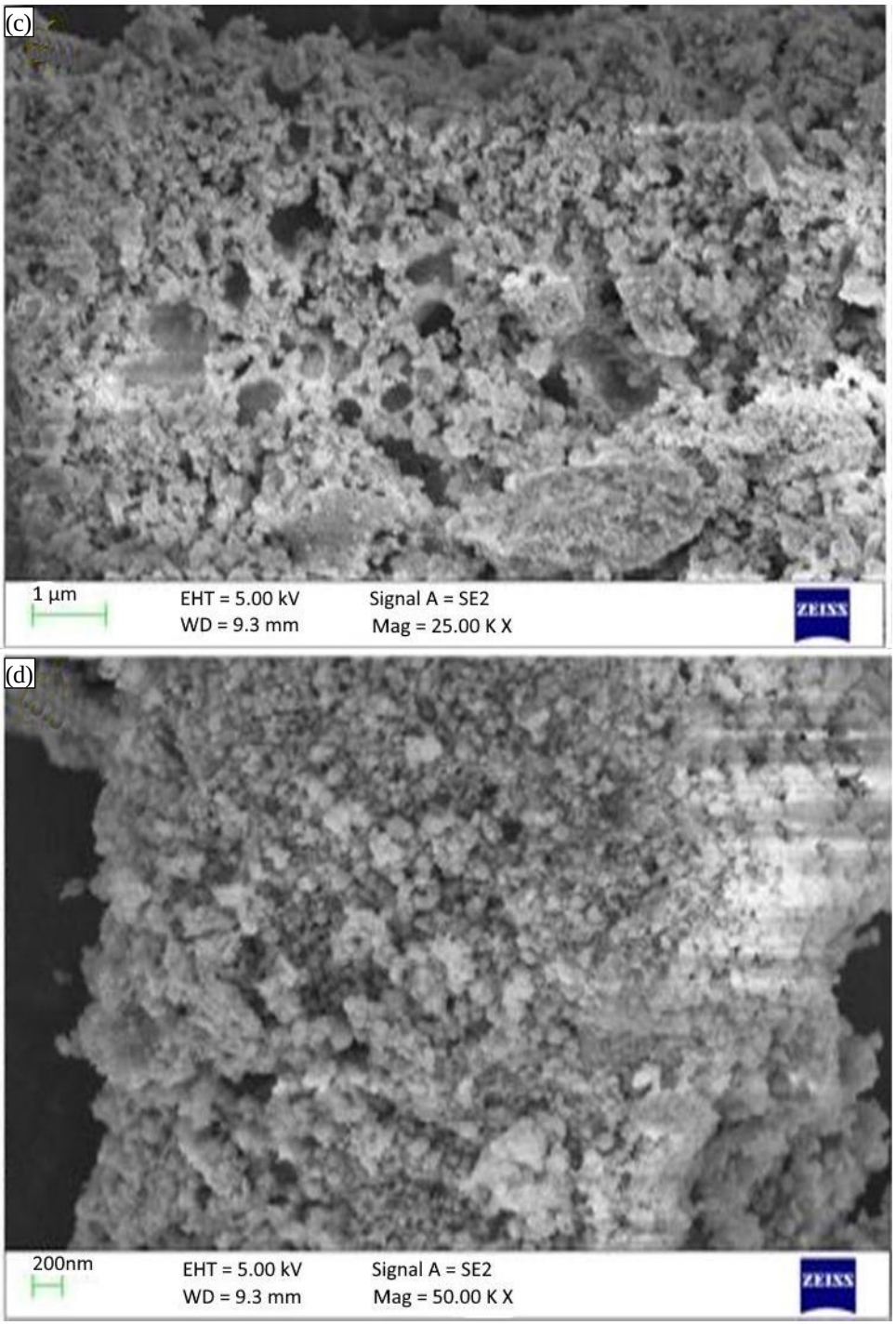


**Figure 3.** Scanning electron microscopy (SEM) images of (a, b) 5% Cu/$CeO_2$ ($Ce_{0.95}Cu_{0.05}O_2$) and (c, d) $CeO_2$ catalysts.

**Ultraviolet-Visible Absorption Studies**

The transmitted peak shifts from a shorter wavelength to a higher wavelength. It represents the thin, single particle size distribution obtained with this production approach.

The ultraviolet-visible (UV-visible) spectra revealed no alternative peak associated with contaminants and structural flaws, confirming that the synthesized nanoparticles are pure $CeO_2$. The absorption wavelength appears to be 329 nm for $CeO_2$ nanoparticles [17].

 

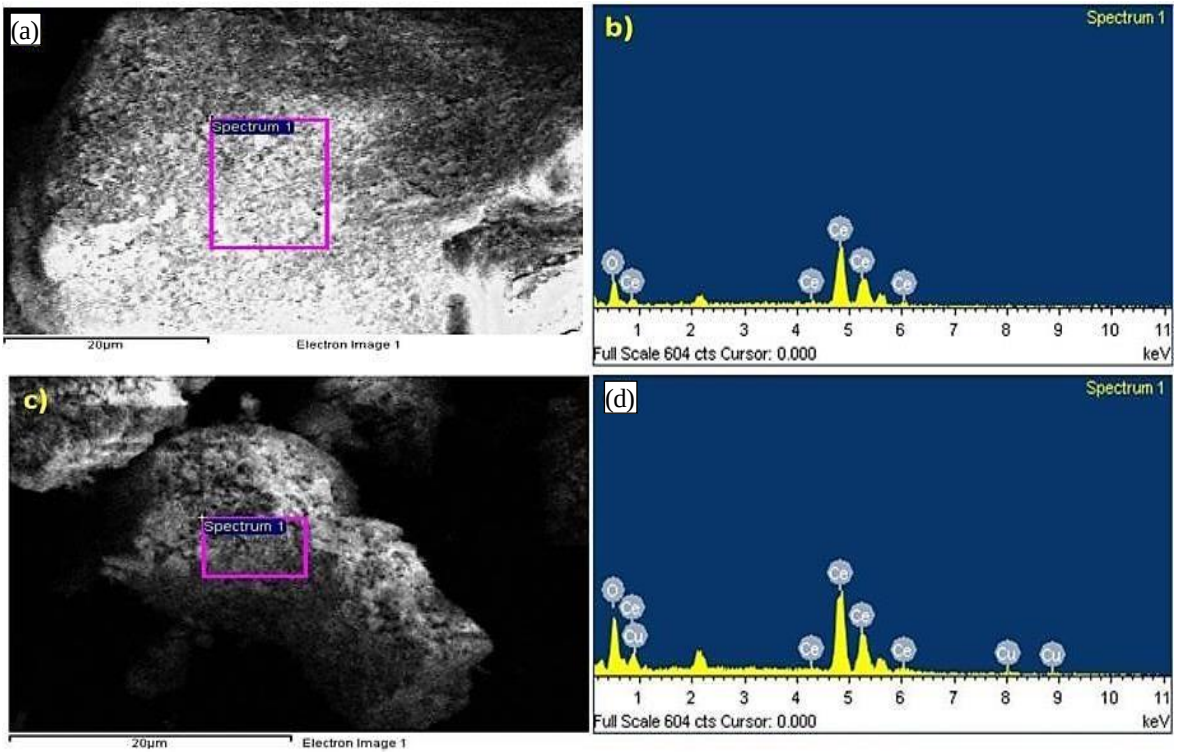


**Figure 4.** Energy-dispersive X-ray (EDAX) images of (a, b) $CeO_2$ and (c, d) 5% $Cu/CeO_2$ ($Ce_{0.95}Cu_{0.05}O_2$).

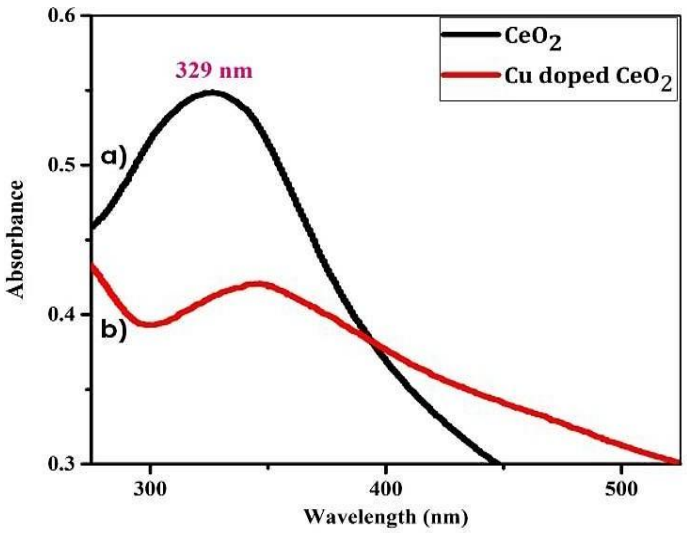


**Figure 5.** Ultraviolet (UV) absorption spectra of (a) $CeO_2$ and (b) Cu doped $CeO_2$.

## PHOTOCATALYSIS STUDIES

The synthesized $Cu/CeO_2$ nanoparticle sample was subjected to photocatalytic studies to investigate its ability to induce UV-induced degradation of Rose Bengal dye and the results were compared to the degradation of the dye in the absence of any catalyst. Several key factors, such as crystal structure, component concentration, and size and shape of the catalytic particles, were found to significantly affect the activity of the photocatalysts that were generated. The efficiency of the photocatalytic degradation process, which was determined by measuring the decolorization of the pollutant sample, was calculated using a UV-visible spectrophotometer. A concentration of 10 ppm of Rose Bengal dye was subjected to degradation using $Cu/CeO_2$ catalyst under UV lamp (11 W) irradiation. Figures 5 and 6 display the UV-

 

induced degradation of Rose Bengal dye without catalyst. Figures 7 and 8 display the graph depicting the UV-induced degradation of Rose Bengal dye by Cu/$CeO_2$.Chromophore depletion causes the dye molecule to gradually absorb less light over time as the intensity of radiation increases, leading to the production of an intermediate product. The degradation efficiency was calculated using Equation (2),

$$Degradation(\%) = \frac{C_O - C}{C_O} \times 100 \quad (2)$$

where $C_0$ and $C$ are the initial and final dye concentrations in the aqueous solution, respectively.

In 60 minutes, the degradation percentage of Rose Bengal dye in the absence of a catalyst was found to be 44.5%, whereas the degradation percentage increased to approximately 82.7% when Cu/$CeO_2$ was used as a catalyst. These results indicate that the catalyst was more efficient in promoting the degradation of the dye than the dye alone. The Lagergren rate equation is often utilized to describe the breakdown of adsorbate from an aqueous solution. Specifically, the first-order rate of the Lagergren equation can be represented by Equation (2)

$$k = -In\frac{C}{C_O} \quad (3)$$

The kinetic constant, $k$, was used in the equation, and a graph of $-\ln(C/C_0)$ versus the duration of irradiation (in minutes) is shown in Figure 8(a) and b) to examine the rate constants of the reaction.

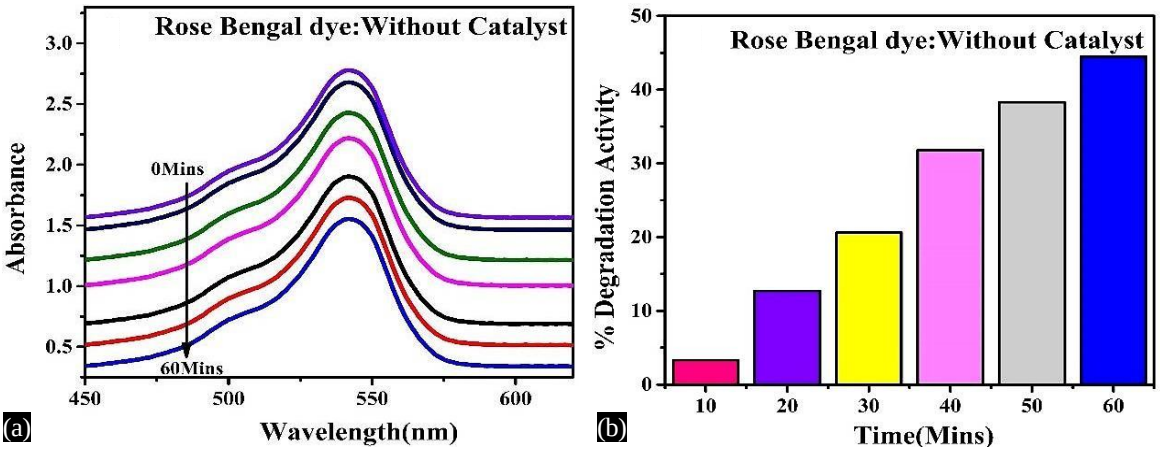


**Figure 6.** (a) Ultraviolet (UV)-visible spectra of Rose Bengal dye. (b) Percentage degradation of Rose Bengal.

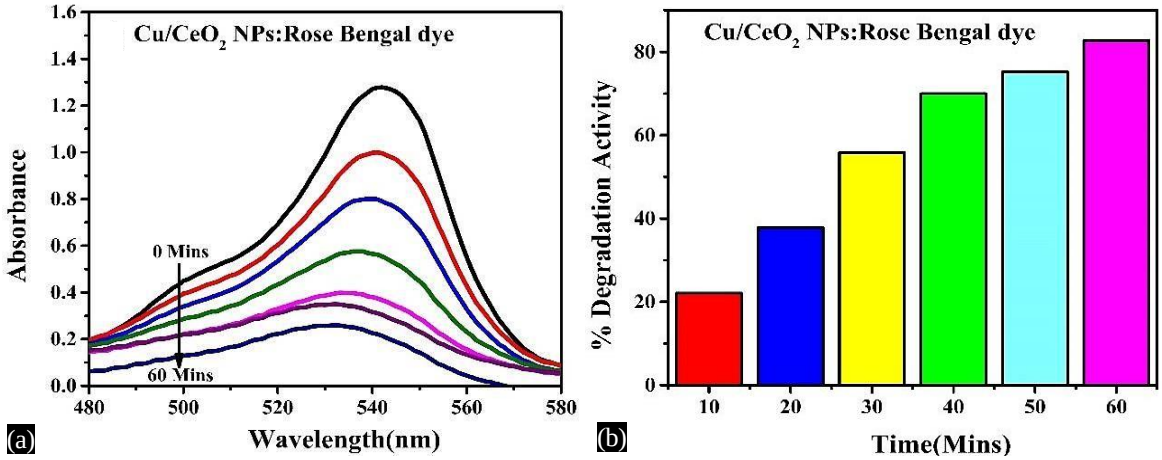


**Figure 7.** (a) Ultraviolet (UV)-visible spectra of Rose Bengal using Cu/$CeO_2$ nanoparticles. (b) Degradation graph of Rose Bengal using Cu/$CeO_2$ nanoparticles.

 

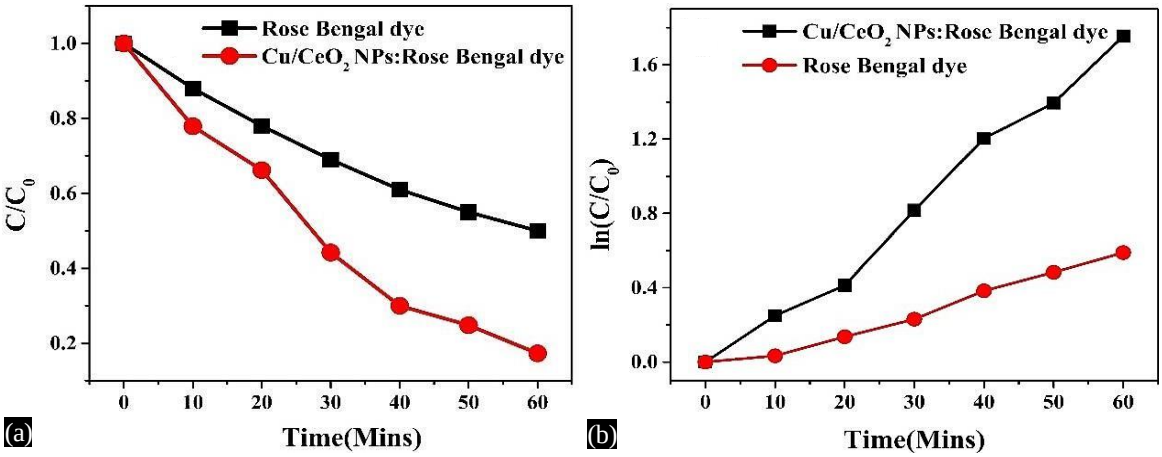


**Figure 8.** (a) ($C/C_0$) versus time interval and (b) plot of $-\ln(C/C_0)$ versus time interval for Rose Bengal dye by using $Cu/CeO_2$ nanoparticles.

**Table 2.** Photocatalytic activity of Rose Bengal dye using $Cu/CeO_2$ nanoparticles.

| Sample | Degradation Efficiency | $k$ ($min^{-1}$) | $R^2$ |
|---|---|---|---|
| Rose Bengal | 44.5 | 0.0113 | 0.9962 |
| Rose Bengal-$Cu/CeO_2$ | 82.7 | 0.0305 | 0.9936 |

The final results of kinetic rate and experimental values for $k$ and $R^2$ are mentioned in Table 2. The degradation process of Rose Bengal and Rose Bengal dye (without catalyst) through photocatalysis using $Cu/CeO_2$ nanoparticles catalyst resulted in kinetic constants ($k$) of 0.0305 and 0.0113 $min^{-1}$, respectively [18, 19]. The kinetic parameter displayed the Rose Bengal dye photo catalytically decomposed in presence of UV light when $Cu/CeO_2$ was used as catalyst.

## CONCLUSION

In an effort to investigate the degradation of Rose Bengal dye, we generated significant surface area metal oxide $CeO_2$ and Cu-doped $CeO_2$ nanoparticles. $CeO_2$ and $Cu/CeO_2$ are both present in the nanoparticles, and when they were synthesized individually, XRD analysis showed that they had a face-centered cubic crystal structure with the space group Fm-3m, $Ce^{4+}$ ions at tetrahedral sites, and $O^{2-}$ ions at octahedral lattice sites. The average particle size varies between 20.73 and 23.22 nm resulting in a substantial surface area, according to the SEM image for $CeO_2$ and $Cu/CeO_2$ NPs. In photocatalytic studies the obtained catalyst exhibited significantly 82.7% degradation of Rose Bengal dye when compared to dye without catalyst. $Cu/CeO_2$ nanoparticles were used as a catalyst in the photocatalytic degradation of Rose Bengal and Rose Bengal dye (without catalyst), which resulted in kinetic constants ($k$) of 0.0305 and 0.0113 $min^{-1}$, respectively.

## REFERENCES

1. Tsunekawa S, Fukuda T, Kasuya A. Blue shift in ultraviolet absorption spectra of monodisperse $CeO_{2x}$ nanoparticles. J Appl Phys. 2000; 87: 1318–1321.
2. Afzal S, Quan X, Lu S. Catalytic performance and an insight into the mechanism of $CeO_2$ nanocrystals with different exposed facets in catalytic ozonation of *p*-nitrophenol. Appl Catal B Environ. 2019; 248: 526–537.
3. Shuang L, Xiaodong W, Duan W, Rui R. Ceria-based catalysts for soot oxidation: a review. J Rare Earth. 2015; 33: 567–590.
4. Zhao B, Shao Q, Hao L, Zhang L, Liu Z, Zhang B, Ge S, Guo Z. Yeast template synthesized Fe-doped cerium oxide hollow microspheres for visible photodegradation of acid orange 7. J Colloid and Interface Sci. 2018; 511: 39–47.

 

5. Kumari K, Aljawfi RN, Vij A, Chae KH, Hashim M, Alvi PA, Kumar S. Band gap engineering, electronic state and local atomic structure of Ni doped $CeO_2$ nanoparticles. J Mater Sci Mater Electron. 2019; 30: 4562–4571.
6. Alla SK, Komarala EVP, Mandal RK, Prasad NK. Structural, optical and magnetic properties of Cr-substituted $CeO_2$ nanoparticles. Mater Chem Phys. 2016; 182: 280–286.
7. Zhang D, Qian Y, Shi L, Mai H, Gao R, Zhang J, Yu W, Cao W. Cu-doped $CeO_2$ 15 spheres: synthesis, characterization, and catalytic activity. Catal Commun. 2012; 12: 164–168.
8. Obaiah GO, Shivaprasad KH, Mylarappa M. Synthesis and structural characterization of undoped $CeO_2$ and Pd doped $CeO_2$ for photocatalytic studies under sunlight and UV-light irrasiation. Int J Adv Sci Technol. 2020; 29 (3s): 1436–1453.
9. Saravanan R, Karthikeyan N, Govindan S, Narayanan V, Stephen A. Photocatalytic degradation of organic dyes using ZnO/$CeO_2$ nanocomposite material under visible light. Adv Mater Res. 2012; 584: 381–385.
10. Zhou G, Shah PR, Montini T, Fornasiero P, Gorte RJ. Oxidation enthalpies for reduction of ceria surfaces. Surf Sci. 2007; 601: 2512–2519.
11. Lanje AS, Sharma SJ, Pode RB, Ningthoujam RS. Synthesis and optical characterization of copper oxide nanoparticles. Adv Appl Sci Res. 2010; 1: 36–40.
12. Wongpisutpaisan N, Charoonsuk P, Vittayakorn N, Pecharapa W. Sonochemical synthesis and characterization of copper oxide nanoparticles. Energy Procedia. 2011; 9: 404–409.
13. Nasir M, Bagwasi S, Jiao Y, Chen F, Tian B, Zhang J. Characterization and activity of the Ce and N co-doped $TiO_2$ prepared through hydrothermal method. Chem Eng J. 2014; 236: 388–397.
14. Magdalane CM, Kaviyarasu K, Judith Vijaya J, Jayakumar C, Maaza M, Jeyaraj B. Photocatalytic degradation effect of malachite green and catalytic hydrogenation by UV-illuminated $CeO_2$/CdO multilayered nanoplatelet arrays: investigation of antifungal and antimicrobial activities. J Photochem Photobiol B Biol. 2017; 169: 110–123.
15. Rajendran S, Khan MM, Gracia F, Qin J, Gupta VK, Arumainathan S. $Ce^{3+}$-ion induced visible-light photocatalytic degradation and electrochemical activity of ZnO/$CeO_2$ nanocomposite. Sci Rep. 2016; 6: Article 31641.
16. Arshad T, Khan SA, Faisal M, Shah Z, Akhtar K, Asiri AM, Ismail AA, Alhogbi BG, Khan SB. Cerium based photocatalysts for the degradation of acridine orange in visible light. J Mol Liq. 2017; 241: 20–26.
17. Zhang F, Chan S-W, Spanier JE, Apak E, Jin Q, Robinson RD, Herman IP. Cerium oxide nanoparticles: size-selective formation and structure analysis. Appl Phys Lett. 2002; 80: 127–129.
18. Obaiah GO, Shivaprasad KH, Bhat KS, Hegde MS, Mylarappa M. Development and catalytic application of palladium doped titania ($Ti_{0.98}Pd_{0.02}O_2$) through low temperature solution combustion method. Adv Sci Lett. 2018; 24 (8): 6004–6007.
19. Soni S, Kumar S, Dalela B, Kumar S, Alvi PA, Dalela S. Defects and oxygen vacancies tailored structural and optical properties in $CeO_2$ nanoparticles doped with $Sm^{3+}$ cation. J Alloys Compounds. 2018; 752: 520–531.

 